Ninth International Conference on CFD in the Minerals and Process Industries
CSIRO, Melbourne, Australia
10–12 December 2012

LOCALISED INDUCEMENT OF BUBBLE SURFACE MOBILITY DUE TO MOTION OF A NEARBY PARTICLE

David I. VERRELLI

CSIRO Process Science and Engineering, Clayton, Victoria 3168, AUSTRALIA
E-mail address: David.Verrelli@csiro.au

ABSTRACT

Bubbles found in nature or in industrial systems are often presumed to have immobile surfaces (*i.e.* a 'no-slip' boundary condition), due to surfactant adsorption. Even trace amounts of surfactants in the bulk liquid can result in effective immobilisation, because of the preferential partitioning of surfactants at the interface.

In froth flotation, used to separate valuable minerals from waste 'gangue', interaction of bubbles with particles is modelled to predict the possibility of achieving attachment. The modelling often presumes a completely immobile bubble surface — although the alternative limiting condition of a fully mobile bubble surface ('full slip' boundary condition) is occasionally investigated.

From recent experimental observations of a particle falling onto a submerged bubble it was concluded that the interface was partially mobile. A closer inspection of the data revealed that a transition from the immobile to (partially) mobile state may be occurring locally.

It is known that flow of liquid over the surface of a rising bubble can sweep adsorbed surfactants to the rear of the bubble, forming a 'stagnant cap'. A similar principle could apply, locally, as liquid is squeezed out of the gap between a bubble and an approaching particle.

In flotation the particles are often much smaller than the bubbles. The gas–liquid interface can then be approximated as a plane, and analytical solutions for the flow field are known. I derived from these the shear stresses at the bubble's surface in bipolar co-ordinates, for both parallel and perpendicular components of the particle's motion. Both cases attained shear stresses much greater than those required to form a stagnant cap. The tangential particle motion induced stresses that would be sufficient to sweep surfactant out of the interaction zone, thereby locally enhancing the surface mobility.

These new findings quantitatively support the existence of a transition of bubble surface mobility, mediated by motion of a nearby particle, and strongly dependent upon the particle's trajectory.

NOMENCLATURE

- c parameter in bipolar co-ordinates describing distance of particle from bubble surface, equal to $\sqrt{\delta^2 + 2\delta R_\text{p}}$ (*cf.* Brenner, 1961; Chaoui & Feuillebois, 2003)
- d_i density of particle (i=p) or liquid (i=f) or bubble (i=b)
- f_i correction to radial (i=r) or tangential (i=t) drag for microhydrodynamic effects
- $\boldsymbol{g}$ gravitational acceleration
- G_{n+1} Gegenbauer polynomial of degree −½
- h_i metrical coefficient, for conversion between co-ordinate systems: derivative of i-ordinate itself with respect to distance along i-ordinate curve
- $h_\bullet$ metrical coefficient for ξ and η; $h_\xi = h_\eta = \dfrac{\cosh(\eta) - \cos(\xi)}{c} \equiv h_\bullet$
- n summation index
- Q_1 spherical harmonic function (see O'Neill, 1964)
- r radial position in spherical co-ordinates, with origin at bubble centre; especially used to describe location of particle centre
- R_b bubble radius
- R_p particle radius
- t time
- T parameter related to the viscous relaxation time
- $\boldsymbol{u}_i$ particle velocity in the i-direction
- $\boldsymbol{u}_\text{S}$ Stokes velocity
- U velocity of bubble, or particle, or streaming bulk liquid
- U_0, U_2 spherical harmonic functions (see O'Neill, 1964)
- $\boldsymbol{v}_i$ local fluid velocity in the i-direction
- w_1 spherical harmonic function (see O'Neill, 1964)
- x fractional mobility of bubble surface
- z elevation off plane, a position ordinate in circular cylindrical co-ordinates

- δ gap thickness, the shortest distance between particle and bubble surfaces, at a given time
- η ordinate parameterising a family of circles in a pair of coaxial groups centred on the z-axis at $\pm c\left|\coth(\eta)\right|$, a position ordinate in bipolar co-ordinates
- θ azimuthal angle, or 'longitude', measured around from x–z plane (anticlockwise looking down z-axis), used as position ordinate in circular cylindrical co-ordinates and bipolar co-ordinates
- Θ azimuthal angle, used as position ordinate in spherical co-ordinates
- μ dynamic viscosity of liquid phase
- ξ ordinate parameterising a family of circular arcs of revolution symmetrical about the x–y plane and z-axis, and passing through $z = +c$ and $z = -c$, a position ordinate in bipolar co-ordinates
- ρ radial distance in x–y plane, used as position ordinate in circular cylindrical co-ordinates
- σ surface tension of gas–liquid interface

τ_{ij} shear stress: summation of stress due to momentum transfer in i direction due to j motion and the converse

υ_n a function of particle velocity and position; written as U_n by Brenner (1961)

φ polar angle, or 'latitude', as position ordinate in spherical co-ordinates, measured out from vertical axis, with origin at bubble centre; especially used to describe location of particle centre

ψ stream function

The convention of Happel & Brenner (1983) is adopted here for naming the bipolar co-ordinates: see **Figure 1**. *Caution*: Brenner (1961) and a number of other researchers use the opposite nomenclature!
Some authors use the reciprocal of the metrical coefficients (Happel & Brenner, 1983), termed "scale factors".

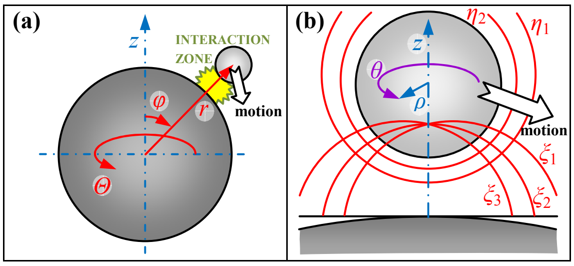

Figure 1: Co-ordinate systems used. **(a)** Spherical co-ordinates to describe particle position and motion. **(b)** Bipolar or circular cylindrical co-ordinates to describe fluid motion and stresses in the interaction zone. The bubble surface is approximated locally as a plane.

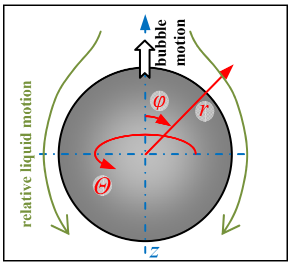

Figure 2: Schematic illustrating the co-ordinates, and relative fluid motions, for a bubble rising through a quiescent liquid.

INTRODUCTION

In describing the interaction of two solid particles the boundary condition at the respective surfaces is obviously the 'no slip' condition. When one (or both) of the objects is fluid, the appropriate boundary condition becomes open to question. Herein behaviour at the surface of a bubble is investigated when it is approached by a solid particle.
Such considerations are directly relevant to a wide variety of processes, ranging from surf zone patch dynamics in the natural aquatic environment (Talbot *et al.*, 1990), to bubble–particle interaction and attachment in industrial operations — *e.g.* dissolved air flotation (DAF) in water and wastewater treatment, froth flotation in mineral processing, and deinking flotation (Nguyen & Schulze, 2004) — to experimental research carried out in devices such as the atomic force microscope (Manor, 2010). Moreover, the insights can be extended to application in other situations in which a dispersed fluid phase is subject to shear due to the local flow field, such as in microfluidics (Bremond *et al.*, 2008).
The interaction of bubbles with either particles or other bubbles is often of interest due to the possibility of achieving attachment or coalescence, respectively. In froth flotation, used to separate valuable minerals from waste 'gangue', modelling often presumes a completely immobile bubble surface — although the alternative limiting condition of a fully mobile bubble surface ('full slip' boundary condition) is occasionally investigated (see Nguyen & Schulze, 2004).
When considering a bubble rising through a liquid, as in **Figure 2**, it is accepted that surfactant can be swept to the rear of the bubble, creating a more mobile surface at the leading face of the bubble, and a less mobile (*i.e.* more immobile) interface at the back of the bubble, known as the "stagnant cap" (Clift *et al.*, 1978; Li & Mao, 2001).
Based on experimental observations I hypothesise that shear at the bubble's surface due to the particle's motion can induce local mobilisation of the gas–liquid interface. This is explored first by consideration of the fractional mobility for which the transient velocity of the particle obtained by computational prediction matches the experimentally observed behaviour. Second, the shear stress experienced at the bubble surface in two different scenarios is computed: for a particle approaching the apex of the bubble, and for a particle approaching off-axis, and 'sliding' over the bubble's surface. These are compared with the shear stress on a rising bubble which might be expected to give rise to a stagnant cap due to distribution of surfactant as a function of the polar angle, φ.

EXPERIMENTAL METHOD

The original experimental measurements were made by allowing spherical glass beads to settle under the action of gravity onto a stationary bubble, held captive at the end of a capillary, the whole being carried out in a quiescent medium of purified water at ambient temperature and pressure in the *CSIRO Milli-Timer* apparatus (Verrelli & Koh, 2010; Verrelli *et al.*, 2011). Although the particles were methylated to render their surfaces relatively hydrophobic, for the case of interest the approach trajectory commences sufficiently far from the vertical axis through the bubble's centre that hydrodynamics prevents the two surfaces from coming close enough for any attractive (surface chemical) forces to take control.
The bubble and particle diameters for the specific case presented herein are approximately 1.26 and 0.141 mm, respectively, both objects being close to perfect spheres.
Further details of the experimental procedure can be found in the references given.

MODEL DESCRIPTIONS

Overall conditions and assumptions

The liquid medium is water, with a density of 1000 kg/m^3, viscosity of 1 mPa.s (Newtonian), and surface tension of 72 mN/m. Industrial flotation cells commonly operate at somewhat elevated temperatures, in which case the viscosity would be reduced. The particle's density is taken as 2450 kg/m^3, consistent with the soda–lime glass *Ballotini* used in the experimental work. The bubble is constituted of air, with a density of practically 0 kg/m^3.

In all of the modelling that follows, the bubble is assumed to be a rigid sphere. No forces arising from surface chemistry are included — they are certainly negligible for large separation distances; their omission even for the smallest gaps, δ, considered herein can be considered an approximation.

All of the microhydrodynamic drag functions suppose that the bubble is much larger than the particle, so that the gas–liquid interface can be treated as locally flat. This is a reasonable assumption, as the bubble is approximately 10 times the size of the particle.

Apart from where explicitly included as a separate term, effects of both fluid inertia and particle acceleration are assumed negligible (*cf.* Verrelli *et al.*, 2012c).

For all shear stress calculations an immobile surface is assumed, which yields an upper limit. The shear stress would be practically zero for a fully mobile gas–liquid interface, assuming the viscosity of the gas phase to be negligible, and likewise for the viscosity of the interface itself (*cf.* Clift *et al.*, 1978; Tan *et al.*, 2009).

Unless otherwise stated, all particle trajectories lie on the meridian of $\Theta = 0$ (for which $\theta = 0$ or π).

Prediction of particle trajectory

The trajectory of a particle as it encounters a bubble is predicted using an algorithm adapted from that originally due to Nguyen, presented by Verrelli *et al.* (2011) and variously applied thereafter (Verrelli *et al.*, 2012a; Verrelli *et al.*, 2012b). The independent variables of r and φ track the particle's centre.

The governing equations are obtained from the Basset–Boussinesq–Oseen (BBO) equation (Nguyen & Schulze, 2004), neglecting the Basset force as particle accelerations are relatively small for the conditions presently studied (Verrelli *et al.*, 2012c). A system of four equations is obtained:

$$\frac{\mathrm{d}u_r}{\mathrm{d}t} = \frac{{u_\varphi}^2}{r} - \frac{f_\mathrm{r}\, u_r + u_\mathrm{S} \cos\varphi}{T}\,, \tag{1a}$$

$$\frac{\mathrm{d}u_\varphi}{\mathrm{d}t} = -\frac{u_r\, u_\varphi}{r} - \frac{f_\mathrm{t}\, u_\varphi - u_\mathrm{S} \sin\varphi}{T}\,, \tag{1b}$$

$$\frac{\mathrm{d}r}{\mathrm{d}t} = u_r\,, \tag{1c}$$

$$\frac{\mathrm{d}\varphi}{\mathrm{d}t} = \frac{u_\varphi}{r} \tag{1d}$$

in which

$$T \equiv \frac{{R_\mathrm{p}}^2 \left(2\, d_\mathrm{p} + d_\mathrm{f}\right)}{9\,\mu}\,, \tag{2}$$

$$\boldsymbol{u}_\mathrm{S} \equiv \frac{2\, {R_\mathrm{p}}^2 \left(d_\mathrm{p} - d_\mathrm{f}\right)}{9\,\mu}\, \boldsymbol{g}\,, \tag{3}$$

$$f_\mathrm{r} = x\, f_\mathrm{r,mobile} + (1-x)\, f_\mathrm{r,immobile}\,, \tag{4}$$

$$f_\mathrm{t} = x\, f_\mathrm{t,mobile} + (1-x)\, f_\mathrm{t,immobile}\,, \tag{5}$$

with the drag correction functions $f_{\mathrm{r},\ldots}$ and $f_{\mathrm{t},\ldots}$ for a perfectly mobile or immobile bubble surface estimated respectively from the four rational approximation formulæ of Nguyen & Evans (see Nguyen & Schulze, 2004) that were used previously (Verrelli *et al.*, 2011).

An indication of values of the various components of force implicit in equations 1a and 1b is presented in a companion paper (Verrelli *et al.*, 2012c).

I have made several notable changes to the equations and their solution since the previously described work (*cf.* Verrelli *et al.*, 2012c).

(i) The drag correction functions f_r and f_t are composed as interpolations between the two limiting cases of perfectly mobile and perfectly immobile bubble surfaces, based on the fractional bubble surface mobility, x, which in turn is a function of the gap, δ. (The gap, δ, also indirectly accounts for particle speed.) The function x was adjusted through a trial-and-error process to obtain a predicted velocity profile concordant with the empirically observed one.

(ii) The governing system of equations was found to constitute a 'stiff system' whenever the predicted particle trajectory encountered small gaps, for which the microhydrodynamic resistances increased sharply. Hence greatly improved computational efficiency was obtained by swapping from a Runge–Kutta algorithm to a variable-order solver (implemented at order 5) based on numerical differentiation formulæ that is well-suited to stiff problems — namely the `ode15s` routine in *MATLAB* (Shampine & Reichelt, 1997).

(iii) Tolerances in solving the differential equations were tightened. The solution components were required to have fractional error of less than approximately 10^{-8} for all components greater than 1×10^{-11} in magnitude.

(iv) The arguments of f_r and f_t were not altered for small gaps, less than 10 nm.

Limiting case of axial approach at small gaps

When the gap is small, the lubrication approximation applies. The specific case of a spherical solid approaching a plane wall in a quiescent fluid, under the action of gravity, was derived by Taylor (presented by Hardy & Bircumshaw, 1925). After correction for buoyancy, Taylor's equation is

$$\delta = \delta\big|_{t=0} \exp\!\left(\frac{-2(d_\mathrm{p} - d_\mathrm{f})\, R_\mathrm{p}\, g}{9\,\mu}\, t\right), \tag{6}$$

from which it can be found that

$$u = u_r = \frac{\mathrm{d}\delta}{\mathrm{d}t} = \frac{-2(d_\mathrm{p} - d_\mathrm{f})\, R_\mathrm{p}\, g}{9\,\mu}\, \delta \tag{7}$$

(see also Parkinson, 2010). It is apparent that for small gaps the particle's velocity is directly proportional to the gap.

Connexion between surface shear stress and mobility

The shear stress at a free surface must be balanced by other forces, which typically arise from a gradient in surface tension, due to a non-uniform distribution of surface active agents ("surfactants") at the interface. The relationship is given by (Leal, 2007)

$$\tau_{r\varphi}\big|_{r=R_\mathrm{b}} = -\frac{1}{R_\mathrm{b}} \frac{\mathrm{d}\sigma}{\mathrm{d}\varphi}\,. \tag{8}$$

The surfactants can be intentionally-added detergents, 'opportunistic' organic species, or other molecules. A decent surfactant can readily depress the static surface tension of water from its pure value of ~72–73 mN/m to, say, 60 mN/m even at very low (sub-micromolar) concentrations in the bulk (Tan *et al.*, 2009; Tan *et al.*, 2005).

For a bubble rising through a stagnant liquid, as in **Figure 2**, the manifestation of different surface mobility due to the relative liquid motion is a longstanding theory. The analytical equations for this situation are readily available, and so it serves as a useful benchmark for the more complicated scenarios to follow.

For a rising bubble the change in surface tension from the nose to the tail of the bubble can be calculated from equation 8 by integrating the shear stress, if it is known:

$$\Delta\sigma = -R_\mathrm{b}\int_0^\pi \tau_{r\varphi}\Big|_{r=R_\mathrm{b}} .\mathrm{d}\varphi \,. \tag{9}$$

Thus a change in surface tension of order 10 mN/m, together with R_b, gives a preliminary indication of the magnitude of shear stresses that could be expected to induce localised mobilisation of the bubble surface by depletion of surfactant in the interaction zone.

For a stationary bubble approached by a particle, the integration is performed along a line at the bubble surface in the bubble–particle interaction zone, *viz*.

$$\Delta\sigma = \int_0^{R_\mathrm{p}} \tau_{\rho z}\Big|_{z=0} .\mathrm{d}\rho \,. \tag{10}$$

The interaction zone will have a diameter similar to that of the particle itself. For simplicity, herein $\Delta\sigma$ is only calculated for the forward half of the interaction zone.

Shear stress on surface of a rising bubble

The formula for evaluating the shear stress acting at the surface of a rising bubble with an immobile interface is presented in standard texts (Bird *et al.*, 1960), *viz*.

$$\tau_{r\varphi} = \frac{-3\,\mu\,U\sin(\varphi)}{2\,R_\mathrm{b}}\left(\frac{R_\mathrm{b}}{r}\right)^4 , \tag{11}$$

and at the bubble's surface this reduces to

$$\tau_{r\varphi}\Big|_{r=R_\mathrm{b}} = \frac{-3\,\mu\,U\sin(\varphi)}{2\,R_\mathrm{b}} \,. \tag{12}$$

Note that the shear stress experienced at the immobile interface is the same irrespective of whether the bubble rises through a quiescent medium, or whether the liquid streams past a stationary bubble — the difference is merely in the frame of reference chosen.

Equations 11 and 12 can also be obtained by differentiation of the velocity components v_r and v_φ in spherical co-ordinates for uniform translation of a sphere in uniform flow, parallel to the flow direction (see Bird *et al.*, 1960; Happel & Brenner, 1983), given that (Bird *et al.*, 1960)

$$\tau_{r\varphi} = \tau_{\varphi r} = -\mu\left[r\frac{\partial}{\partial r}\left(\frac{v_\varphi}{r}\right) + \frac{1}{r}\left(\frac{\partial v_r}{\partial\varphi}\right)\right]. \tag{13}$$

The value of U has been taken as the terminal rise velocity of a bubble of the given diameter. This could, in principle, be estimated using a limiting analytical formula or an empirical correlation: for example, reference to the formula for the Stokes velocity in equation 3 indicates that the shear stress will vary approximately as

$$\tau_{r\varphi}\Big|_{r=R_\mathrm{b}} \mathrel{\dot{\propto}} R_\mathrm{b}\left(d_\mathrm{f} - d_\mathrm{b}\right)\sin(\varphi)\,g \tag{14}$$

at small Reynolds numbers.

The work of Savic and other researchers indicates that stagnant cap effects first become obvious for an Eötvös number (or Bond number), $g\Delta d(2R_\mathrm{b})^2/\sigma$, of ~9, at which a 10 % enhancement in the terminal rise velocity may be observed (Clift *et al.*, 1978). For an air bubble in water this corresponds to a diameter of approximately 8 mm, for which Stokes' equation is not appropriate. With reference to the chart presented by Clift *et al.* (1978), U is ~0.22 m/s. This yields a Reynolds number of 1760, which is much larger than would ideally be allowed for given the assumptions implicit in equation 12 (*cf.* Clift *et al.*, 1978); nevertheless, it seems to be a common compromise of precision for the sake of practicality (*e.g.* Leal, 2007).

The change in surface tension that could be achieved in this scenario is estimated by substituting equation 12 into equation 9, whence

$$\Delta\sigma = 3\,\mu U \,. \tag{15}$$

Shear stress on surface of a bubble for particle exhibiting motion perpendicular to bubble's surface

For a sphere moving perpendicular to a rigid, immobile planar surface, the full flow field was derived by Brenner (1961) in terms of a stream function, *viz*.

$$\psi = \frac{\sum_{n=1}^{\infty} \upsilon_n(\eta)\,G_{n+1}(\xi)}{\left(c\,h_\bullet\right)^{3/2}} , \tag{16}$$

in which the υ_n are complicated functions of particle velocity and position, while G_{n+1} is a Gegenbauer polynomial of degree −½. The summation was evaluated up to n = 100.

The stream function is expressed in bipolar co-ordinates*, so it would be most convenient to evaluate the shear stress in this domain, if the appropriate formula were known. The formula could not be found in the literature, and therefore was derived from first principles, following the guidance in Happel & Brenner (1983), to obtain

$$\begin{aligned}\tau_{\xi\eta}\Big|_{\eta=0} = \tau_{\eta\xi}\Big|_{\eta=0} &= -\mu\,h_\bullet\,\frac{\partial v_\xi}{\partial\eta}\bigg|_{\eta=0} \\ &= +\mu\,h_\bullet\,\frac{\partial}{\partial\eta}\left(\frac{h_\bullet^{\,2}}{\sin(\xi)}\frac{\partial\psi}{\partial\eta}\right)\bigg|_{\eta=0}\end{aligned} \,. \tag{17}$$

Mathematica version 8.0.1.0 (Wolfram Research) was used to perform the calculations. *MATLAB* version 7.12.0.635 (R2012a) (The MathWorks) was used for subsequent processing. The appropriate input velocity and gap pairs were obtained using the methodology described under 'Prediction of particle trajectory' for a particle dropping along the z-axis (φ = 0).

At the bubble's surface, $\tau_{\eta\xi}$ has the same magnitude as $\tau_{\rho z}$, but the opposite sign.

The alternative technique of mapping ψ to circular cylindrical co-ordinates, and then differentiating twice as *per* (Brenner, 1961)

$$v_\rho = \frac{1}{\rho}\frac{\partial\psi}{\partial z} \tag{18a}$$

* Sometimes called "bispherical co-ordinates" (*e.g.* O'Neill, 1964).

$$v_z = -\frac{1}{\rho}\frac{\partial \psi}{\partial \rho} \tag{18b}$$

and (Bird *et al.*, 1960)

$$\tau_{\rho z} = \tau_{z\rho} = -\mu\left[\frac{\partial v_z}{\partial \rho} + \frac{\partial v_\rho}{\partial z}\right], \tag{19}$$

using *Mathematica* did not meet with success — neither using analytical methods nor with numerical differentiation.

Shear stress on surface of a bubble for particle exhibiting motion both parallel and perpendicular to bubble's surface

Under the limiting condition of creeping flow, the linear form of the governing equations allows the fluid flow field for a mixture of simultaneous particle translations and rotations to be obtained by a simple arithmetic summation of the individual behaviours for elementary motions (Goldman *et al.*, 1967; O'Neill, 1964; Pasol *et al.*, 2006). Although creeping flow could not strictly be said to exist at all times in the presently investigated scenarios, and is not an inherent feature of Oseen's derivation (Happel & Brenner, 1983), it becomes a fair simplification especially as the gap is reduced.

For the present purposes, therefore, it suffices to estimate the total shear stress from the individual contributions assuming firstly pure radial motion and secondly pure tangential motion of the particle with respect to the bubble's surface.

Shear stress arising from perpendicular component of motion

Following the foregoing argument, the shear stress for purely radial motion presented in equations 16 and 17 can be used to estimate the contribution of this motion for the mixed case.

Shear stress arising from parallel component of motion

Naïve estimates

Naïve estimates of the peak shear stress at the surface can be obtained by treating the system as if it were two parallel plates, whence (Bird *et al.*, 1960)

$$\tau_{\text{naive}} = -\mu\frac{\Delta v}{\Delta r} = -\mu\frac{U}{\delta}\,. \tag{20}$$

Rigorous estimates

The full flow field for purely tangential motion of a sphere beside a plane was derived by O'Neill (1964)[†] in terms of components of the velocity vector in circular cylindrical co-ordinates, *viz*.

$$v_\rho = \frac{U}{2}\left(\frac{\rho Q_1}{c} + U_2 + U_0\right)\cos(\theta)\,, \tag{21a}$$

$$v_\theta = \frac{U}{2}\left(U_2 - U_0\right)\sin(\theta)\,, \tag{21b}$$

$$v_z = \frac{U}{2}\left(\frac{z Q_1}{c} + 2w_1\right)\cos(\theta)\,, \tag{21c}$$

in which Q_1, U_0, U_2 and w_1 are spherical harmonics, which are complicated functions of the bipolar co-ordinates ξ and η, which in turn depend on the bubble–particle separation (for a given position in space). Each of Q_1, U_0, U_2 and w_1 involve infinite summations, in which the coefficients are usually obtained by linear programming. Herein an alternative explicit method adapted from that of Chaoui & Feuillebois (2003) has been employed, with a starting precision of 500 digits, in order to avoid solving large matrices to find the coefficients. The summations (not shown here) were evaluated up to $n = 100$ for the largest gap and up to $n = 1000$ for the smallest gap considered, with a sliding scale in between. Ideally the summations for the smallest gap would be evaluated up to $n \sim 3000$, but this was computationally prohibitive; nevertheless, the error due to this approximation is estimated to be significantly less than 1 %, and thus satisfactory for the present purposes.

In order to compute the shear stress on the plane, we could evaluate $\tau_{\xi\eta}$ (equivalently, $\tau_{\eta\xi}$) or $\tau_{\rho z}$ (equivalently, $\tau_{z\rho}$). The latter option was found to be less robust, and so the velocity components in bipolar co-ordinates will be required. Again the relevant formulæ could not be found in the literature. Following the guidance in Happel & Brenner (1983) the ξ-component of fluid velocity was derived from first principles as

$$v_\xi = \frac{\left[\cosh(\eta)\cos(\xi) - 1\right]v_\rho \; - \; \sinh(\eta)\sin(\xi)\,v_z}{c\,h_\bullet}\,. \tag{22}$$

Substitution of v_ξ into equation 17 then yields the shear stress at the bubble's surface. Again the calculations are carried out using *Mathematica*. The code was executed in parallel on CSIRO's Burnet cluster.

Input velocity and gap pairs were obtained using the methodology described under 'Prediction of particle trajectory' to enhance the resolution of the experimentally observed trajectory, using an empirical function for x. Using the predicted data was especially important for gap estimation.

RESULTS

Observed and predicted trajectories

The stimulus for the present working hypothesis was the observation of individual particles dropping onto a stationary bubble, which matched neither the predictions for a fully mobile bubble surface nor those for an immobile surface (Verrelli *et al.*, 2011). One of those interactions is re-examined below.

The observed particle trajectory is indicated in **Figure 3**, coloured according to its instantaneous speed. This is compared against the predicted trajectories for the limiting cases of a fully immobile (x=0) or fully mobile (x=1) bubble surface. The hybrid case is intermediate, and is discussed below.

The respective particle speeds as functions of polar angle are plotted separately in **Figure 4**. Previously it was concluded that the observed behaviour lay "intermediate" to that of the 'no slip' and 'full slip' cases (Verrelli *et al.*, 2011) — *i.e.* partial slip. Upon closer examination it appears rather that the observed particle initially behaves in close accordance with the immobile case, and then abruptly changes to a different mode of motion, more akin to the mobile case.

This suggests that a transition occurs at the bubble surface, from immobile to mobile, due to the particle's approach. This possibility was raised by Lowengrub and

[†] See also Chaoui & Feuillebois (2003) and Pasol *et al.* (2006). All three references contain misprints, so care must be taken.

Cristini (see Leal, 2004) and Manor (2010). (Although the particle does not quite achieve the speeds seen in the mobile case, we might suppose that this is a legacy of the earlier surface immobility. It turns out that the 'memory effect' is actually very short. While bubble deformation has been neglected herein, such action would be expected to affect the particle speed too.)

Through a trial-and-error process a hybrid trajectory was obtained to match the observed behaviour, by specifying x as a function of δ [‡], as shown in **Figure 5**. At large gaps the mobility is taken as zero (although it may merely be close to zero), while for the smallest gaps the mobility approaches unity. The fact that this 'correction' provides the closest match to the observed particle speeds suggests that the particle's approach has indeed induced local mobilisation of the bubble surface. However, for both rigour and improved understanding we look next at the surface shear stresses.

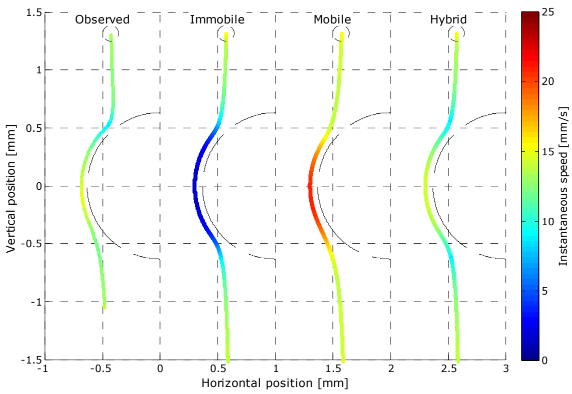

Figure 3: Comparison of observed trajectory and velocity (left) with predictions for immobile & mobile (centre) and partially mobile (right) bubble surfaces. The predicted trajectories are offset, for clarity. Bubble diameter = 1.26 mm. Particle diameter = 141 µm. [An extended version of Fig. 8 from Verrelli *et al*. (2011).]

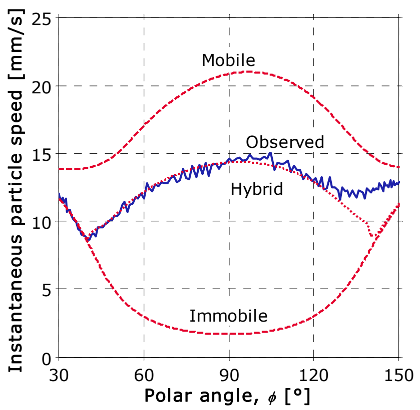

Figure 4: Particle speed as a function of polar angle for the observed and predicted trajectories shown in Figure 3. [An extended version of Fig. 16 from Verrelli *et al*. (2011).]

‡ It is not claimed that x is exclusively a function of δ. Indeed, the working hypothesis is that x is a function of the local shear stress at the bubble's surface. However, the shear stress is difficult to calculate, so δ stands in here as an expedient surrogate parameter.

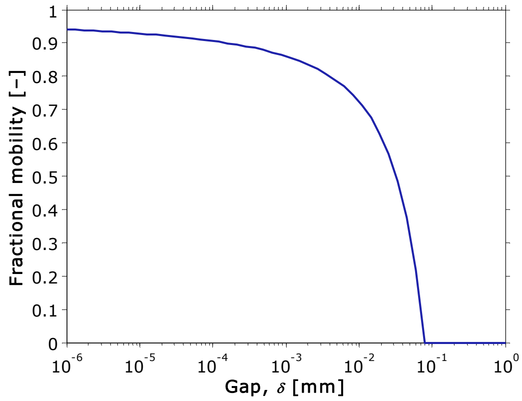

Figure 5: Fractional bubble surface mobility, x, as a function of particle–bubble separation for the "hybrid" case presented in Figure 3 & Figure 4.

Shear stress on a rising bubble

Before estimating the bubble surface shear stresses induced by motion of a nearby particle, let us first evaluate the shear stresses for a rising bubble, in order to obtain a benchmark for subsequent comparison.

For an 8 mm bubble rising at 0.22 m/s the shear stress at the gas–liquid interface, if it were immobile, is given in **Figure 6** as a function of φ. From equation 15 the maximum change in surface tension that could be expected over the surface of the bubble is 0.66 mN/m. This low value suggests that either:

- surfactant coverage at the surface varies from bare to close-packed, but the surfactants used in the literature depress the surface tension only very weakly (unlikely); or
- the surfactants are only slightly depleted from the nose of the bubble under the scenario described (reasonable (*cf.* Leal, 2007; Li & Mao, 2001)); or
- the evaluation of shear stress is a gross underestimate due to inertial effects in the liquid (possible).

For all bubbles in the range 2 to 10 mm in diameter, the terminal rise velocity is approximately the same, at ~0.2 m/s (Clift *et al.*, 1978). Hence, from equation 15 the only difference is not in $\Delta\sigma$ itself, but rather in the distance over which the change in σ occurs.

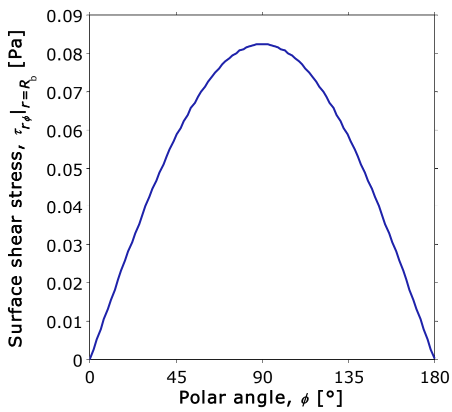

Figure 6: Shear stress on surface of rising bubble of diameter 8 mm, with $U = 0.22$ m/s.

Shear stress for particle approach along z-axis

The simplest form of particle motion that can be described is the axisymmetric case in which the particle moves along the z-axis, and hence the particle velocity has only a radial component.

Shear stress at the bubble surface for a 0.150 mm particle dropping onto a bubble along the vertical axis is given in **Figure 7**. The peak shear stress and particle speed are given in **Figure 8**. The particle speed approaches equation 7 as the gap decreases. Even though the peak shear stress grows at small gaps to be much greater than that found for a rising bubble, it acts over a much shorter distance. Integrating the shear stress at the surface over ρ within the interaction zone according to equation 10 implies a change in surface tension of approximately 0.05 mN/m, which seems inadequate to achieve any perceptible mobilisation of the interface according to the foregoing benchmarks.

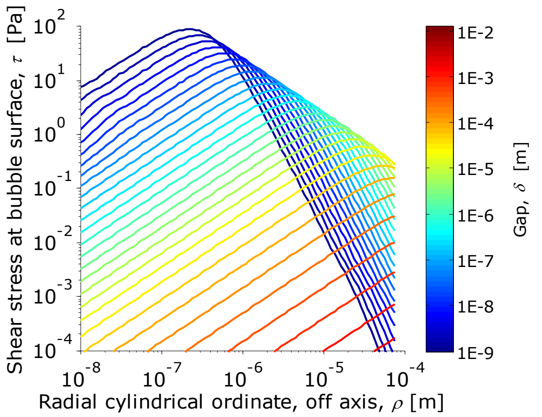

Figure 7: Shear stress at the surface of a large bubble on which a 150 µm particle is impinging at the z-axis, as functions of distance off the z-axis, for various gaps.

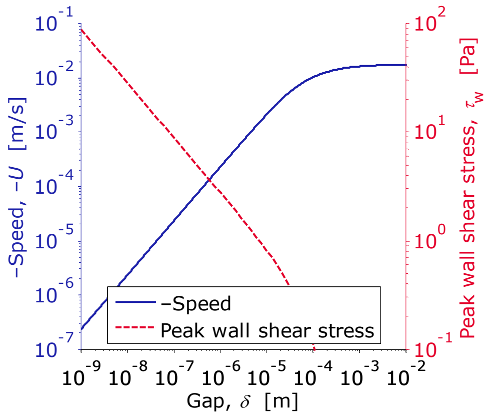

Figure 8: Peak shear stress and transient particle speed, $U = u_r$, as functions of δ for the scenario in Figure 7.

Shear stresses for particle approach off z-axis

The next level of complication is to allow for particle trajectories following from an off-axis approach. As mentioned previously, the flow field can then be obtained as the summation of individual contributions from the radial and tangential components of the motion.

Contribution due to perpendicular movement

Surprisingly, u_r for the off-axis approach depicted in **Figure 3** is only very slightly different from the behaviour of the particle settling toward the bubble's apex described in the previous section, as shown in **Figure 9**, not deviating much from equation 7 at small separations, despite a moderate variation in the radial component of the particle weight force (see Verrelli *et al.*, 2012c). Hence it can be expected that the contribution of this component of the motion for the off-axis approach will be similar in magnitude to the results already presented in **Figure 7** and **Figure 8**.

In contrast, the tangential velocity maintains a large magnitude even down to the smallest gaps encountered in the trajectory of interest. That suggests the motion parallel to the bubble's surface will control the interfacial shear stress.

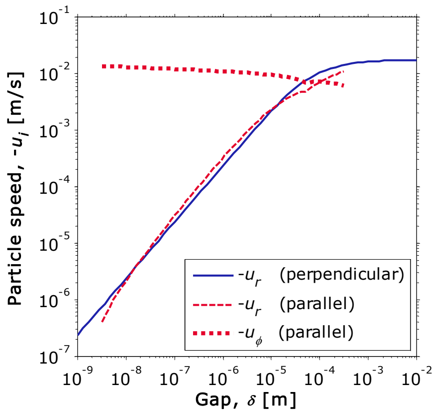

Figure 9: Particle speed components for 150 µm particle approaching along z-axis (perpendicular motion), and 141 µm particle approaching off-axis (predominantly parallel motion) as in Figure 3.

Contribution due to parallel movement

For the parallel movement the fluid flow field is no longer axisymmetric, and hence neither is the shear stress at the bubble surface. For a particle translating along the meridian of $\Theta = 0$, it is intuitive that the maximum shear stress will act along this same meridian, with $\theta = 0$ or $\theta = \pi$. In **Figure 10** this is evaluated for $\theta = 0$ only (*i.e.* 'positive' values of ρ); the stresses for $\theta = \pi$ in equations 21 (*i.e.* 'negative' ρ) are presumed to be an approximate mirror image — at least for the smaller gaps (stresses for the largest gaps being in any case negligible). The shear stresses in **Figure 10** are considerably larger than those in **Figure 7**; moreover they act over a somewhat longer distance.

In **Figure 11** the peak shear stresses are plotted as a function of the gap. These are only slightly lower than the naïve estimates from equation 20.

As shown in the case of the perpendicular approach, it is important to integrate the shear stresses over ρ to get an indication of the change in surface tension that the shear stress could induce. **Figure 12** shows the integrated values as a function of the gap. The total $\Delta\sigma$ for the interaction along the meridian is expected to be approximately double the amount shown in **Figure 12**, which is only for the leading half of the interaction zone, and omits the trailing half. Total $\Delta\sigma$ values of order 10^0 to

10^1 mN/m are predicted. These are clearly a sizeable fraction of the surface tension of water (~72 mN/m), and can be expected to be sufficient to deplete surfactant from the central part of the interaction zone.

It would be expected that the gap at which the fractional mobility was seen to increase sharply in **Figure 5**, *viz*. ~0.05 mm, would correspond to non-negligible values of $\Delta\sigma$ in **Figure 12**, but the estimated values appear negligible. The reason is uncertain at this stage, and further investigation would be beneficial. One possibility is that the adventitious 'surfactants' present in our experimental system depress the static surface tension much more weakly than commercial detergents. Perhaps even trace inorganic ionic species structure at the gas–liquid interface (*cf.* Zimmermann *et al.*, 2010) and stabilise it against shear stresses without decreasing the surface tension much.

A second possibility is that the short time of the interaction (milliseconds) means that the dynamic surface tension should be considered, rather than the static (equilibrium) value. A given concentration of surfactant results in a much smaller reduction in the dynamic surface tension from that of pure water: changes are typically < 1 mN/m (Tan *et al.*, 2005). Hence even the smaller shear stresses may be able to have a significant effect on the local interfacial concentration of surfactant.

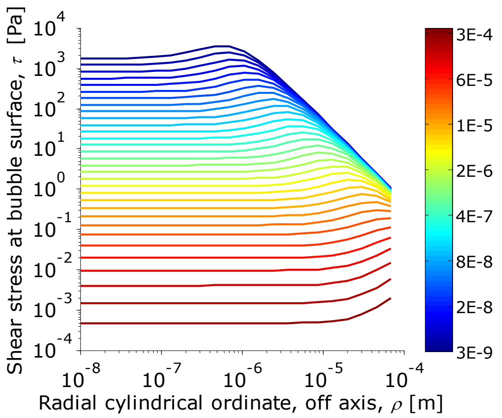

Figure 10: Shear stress at the surface of a large bubble on which a 141 μm particle is impinging off the *z*-axis (as per the 'hybrid' trajectory in Figure 3), as functions of distance off the *z*-axis, for various gaps.

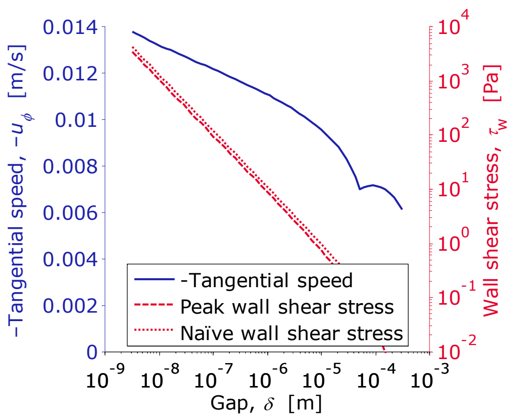

Figure 11: Transient tangential particle speed, u_φ, and corresponding peak shear stress as functions of δ for the scenario in Figure 10.

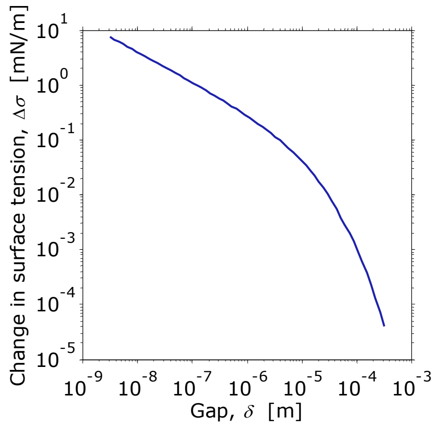

Figure 12: Approximate change in surface tension along meridian of $\Theta = 0$ for $\theta = 0$ as a function of δ for the scenario in Figure 10.

APPLICATION

In many of the applications alluded to in the 'Introduction', such as industrial froth flotation, the bulk fluid flow regime is turbulent. Yet the solutions presented here are based on formulæ derived predominantly for creeping flow.

We may take some reassurance from the fact that even while the bulk fluid flow may be turbulent, at close range the flow is laminar. For example, Liu & Schwarz (2009) estimated the thickness of the boundary layer surrounding a bubble to be approximately 1 mm. Moreover, with regard to the present results, consideration of the particle's tangential speed, u_φ, as a function of particle–bubble separation, δ, presented in **Figure 9** and **Figure 11**, confirms that creeping flow is attained within the gap for small particle–bubble separations, and is a reasonable approximation for the domain of δ treated herein.

As the present work is the first to quantitatively estimate decreases in bubble surface mobility due to nearby particle motion along realistic trajectories in *any* flow regime, it is sensible to commence with a slightly idealised analysis. Notwithstanding these justifications, it would be of interest to extend the analysis to fully account for inertial effects. As discussed by Verrelli *et al.* (2012c), such an objective is difficult to realise by the present approach, and instead a numerical simulation of the flow field based on the Navier–Stokes equations is recommended for that extension. Such a formulation would also allow the effect of other complicating features, such as bubble surface deformation or the adsorption and desorption of surfactant, to be evaluated.

CONCLUSION

Experimental evidence has been presented for localised mobilisation of a bubble's surface due to the motion of a nearby particle. Through numerical simulation a compatible change in the fractional mobility as a function of separation between particle and bubble was deduced.

Equations for the shear stresses acting at the bubble surface due to the liquid flow — caused by the particle's motion nearby — were derived from the exact analytical solutions for the full flow field in the liquid for two ideal cases: perpendicular translation of the particle and parallel translation. The estimates of shear stress were much higher for the latter case; integration in one dimension over the surface showed that this corresponded to a change in surface tension that suggests depletion of opportunistic surfactant molecules in the interaction zone, and hence mobilisation of the interface.

The results are important for fundamental understanding of interfacial dynamics, and have direct implication to micro-scale modelling of the interaction and attachment processes occurring in major industrial processes such as flotation.

ACKNOWLEDGEMENTS

Credit is due to Prof. Anh V. Nguyen for deriving the original algorithms used in the *Chem. Eng. Sci*. paper; several people assisted in the experimental work presented, detailed in the *Chem. Eng. Sci*. paper. I give credit to Dr. Ofer Manor for several helpful tips on computing the shear stresses. I thank Dr. François Feuillebois for graciously answering my questions about implementation of the methods he has published on.

I gratefully acknowledge the ongoing support of CSIRO's Advanced Scientific Computing team, with special thanks to Dr. Tim Ho. I also appreciate ongoing support from Mr. Warren Bruckard, Dr. Peter Koh, and Dr. Phil Schwarz. I thank CSIRO Process Science and Engineering for funding the work. Dr. Yuhua Pan and Dr. Joan Boulanger provided helpful comments on a draft of the manuscript.

REFERENCES

BIRD, R.B., STEWART, W.E. & LIGHTFOOT, E.N., (1960), *Transport Phenomena*, John Wiley & Sons, New York, U.S.A.

BREMOND, N., THIAM, A.R. & BIBETTE, J., (2008), "Decompressing emulsion droplets favors coalescence", *Physical Review Letters*, **100**(2), 024501-024501–024501-024504.

BRENNER, H., (1961), "The slow motion of a sphere through a viscous fluid towards a plane surface", *Chemical Engineering Science*, **16**(3 & 4), 242–251.

CHAOUI, M. & FEUILLEBOIS, F., (2003), "Creeping flow around a sphere in a shear flow close to a wall", *The Quarterly Journal of Mechanics and Applied Mathematics*, **56**(3), 381–410.

CLIFT, R., GRACE, J.R. & WEBER, M.E., (1978), *Bubbles, Drops, and Particles*, Academic Press, New York, U.S.A.

GOLDMAN, A.J., COX, R.G. & BRENNER, H., (1967), "Slow viscous motion of a sphere parallel to a plane wall—I. Motion through a quiescent fluid", *Chemical Engineering Science*, **22**(4), 637–651.

HAPPEL, J. & BRENNER, H., (1983), *Low Reynolds Number Hydrodynamics with Special Applications to Particulate Media*, Martinus Nijhoff, The Hague.

HARDY, W. & BIRCUMSHAW, I., (1925), "Bakerian Lecture. Boundary lubrication. Plane surfaces and the limitations of Amontons' law", *Proceedings of the Royal Society of London. Series A, Containing Papers of a Mathematical and Physical Character*, **CVIII**(745), 1–27.

LEAL, L.G., (2004), "Flow induced coalescence of drops in a viscous fluid", *Physics of Fluids*, **16**(6), 1833–1851.

LEAL, L.G., (2007), *Advanced Transport Phenomena. Fluid Mechanics and Convective Transport Processes* Cambridge University Press Cambridge, England.

LI, X.-J. & MAO, Z.-S., (2001), "The effect of surfactant on the motion of a buoyancy-driven drop at intermediate Reynolds numbers: a numerical approach", *Journal of Colloid and Interface Science*, **240**(1), 307–322.

LIU, T.Y. & SCHWARZ, M.P., (2009), "CFD-based multiscale modelling of bubble–particle collision efficiency in a turbulent flotation cell", *Chemical Engineering Science*, **64**(24), 5287–5301.

MANOR, O., (2010), *Bubbles, Drops and the Physics of their Collisions* [Ph.D. Thesis], Department of Mathematics and Statistics, The University of Melbourne, Melbourne, Australia, 234 pp.

NGUYEN, A.V. & SCHULZE, H.J., (2004), *Colloidal Science of Flotation*, Marcel Dekker, New York, U.S.A.

O'NEILL, M.E., (1964), "A slow motion of viscous liquid caused by a slowly moving solid sphere", *Mathematika*, **11**(1), 67–74.

PARKINSON, L., (2010), *Induction Time and Bubble-Particle Interactions* [Ph.D. thesis], Ian Wark Research Institute, University of South Australia, Adelaide, Australia, 253 pp.

PASOL, L., SELLIER, A. & FEUILLEBOIS, F., (2006), "A sphere in a second degree polynomial creeping flow parallel to a wall", *The Quarterly Journal of Mechanics and Applied Mathematics*, **59**(4), 587–614.

SHAMPINE, L.F. & REICHELT, M.W., (1997), "The MATLAB ODE suite", *SIAM Journal on Scientific Computing*, **18**(1), 1–22.

TALBOT, M.M.B., BATE, G.C. & CAMPBELL, E.E., (1990), "A review of the ecology of surf-zone diatoms, with special reference to *Anaulus australis*", *Oceanography and Marine Biology : an Annual Review*, **28**, 155–175.

TAN, S.N., PUGH, R.J., FORNASIERO, D., SEDEV, R. & RALSTON, J., (2005), "Foaming of polypropylene glycols and glycol/MIBC mixtures", *Minerals Engineering*, **18**(2), 179–188.

TAN, S.N., JIANG, A., LIAU, J.J., GRANO, S.R. & HORN, R.G., (2009), "The surface dilational viscosity of polypropylene glycol solutions and its influence on water flow and foam behavior", *International Journal of Mineral Processing*, **93**(2), 194–203.

VERRELLI, D.I. & KOH, P.T.L., (2010), "Understanding particle–bubble attachment: experiments to improve flotation modelling", *Chemeca 2010*, IChemE in Australia / EA / RACI / SCENZ-IChemE N.Z., Adelaide, Australia.

VERRELLI, D.I., KOH, P.T.L. & NGUYEN, A.V., (2011), "Particle–bubble interaction and attachment in flotation", *Chemical Engineering Science*, **66**(23), 5910–5921 & Supplementary Material.

VERRELLI, D.I., BRUCKARD, W.J., KOH, P.T.L., SCHWARZ, M.P. & FOLLINK, B., (2012a), "Influence of particle shape and roughness on the induction period for particle-bubble attachment", in: RUNKANA, V. & RAI, B. (Eds.), *XXVI International Mineral Processing Congress (IMPC 2012)*, Indian Institute of Mineral Engineers (IIME) and Indian Institute of Metals (IIM), New Delhi, India.

VERRELLI, D.I., KOH, P.T.L., BRUCKARD, W.J. & SCHWARZ, M.P., (2012b), "Variations in the induction period for particle–bubble attachment", *Minerals Engineering*, **36–38**, 219–230.

VERRELLI, D.I., LEE, A., SCHWARZ, M.P. & KOH, P.T.L., (2012c), "Forces arising during bubble-particle interaction", in: WITT, P.J. (Ed.), *Ninth International Conference on Computational Fluid Dynamics in the*

Minerals and Process Industries (CFD2012), CSIRO, Australia, Melbourne, Australia, Accepted October 2012.

ZIMMERMANN, R., FREUDENBERG, U., SCHWEIß, R., KÜTTNER, D. & WERNER, C., (2010), "Hydroxide and hydronium ion adsorption — A survey", *Current Opinion in Colloid & Interface Science*, **15**(3), 196–202.

